Title: Smart Nanotextiles for Communication

Summary

Together with wireless technology, advances in nanotechnology and rapid and scalable synthesis of nanomaterials including the 2D graphene has transformed the realms of biomedical sciences. Recent research in the areas of drug delivery, cancer therapy, bio-sensing and bio-imaging have exploited the unique structural and physiological features of graphene and its different forms. Along with the Graphene, several other nanomaterials including carbon nanotubes (CNTs), make excellent candidates for applications associated with loading of drugs, cellular imaging, sensing other molecules and in-vivo cancer studies due to their biocompatibility and stability. Assimilating from the fundamentals of electromagnetic, wireless communication, medical and material science, a novel concept of nanonetworks was first introduced in 2008, which stems from the concept that a collection of nanodevices have the potential to harness the innate communication capabilities of the human body, thereby allowing them to cooperate and share information. It is anticipated that the advanced healthcare diagnosis can be realised if an efficient communication mechanism and data transfer are established between these nanodevices.

The human body is a good example of a naturally existing communication network. For instance, the nervous system is composed of nerve cells, i.e. neurons that communicate the external stimulus to the brain and enable the communication between different systems by conveying information with a molecular impulse signal known as a spike. The human body needs communication amongst different cells to survive, the proposed intra- and inter-body nanonetworks ensure their stability without mechanically (or physically) disturbing the harmony of the in-built molecular structure of the body. Moreover, in several cases, the medicine technology fails to understand the root cause of the problem but once we have a monitoring network established in our body, we can extract various unknowns and treat them effectively.

The vision of nanoscale networking attempts to achieve the functionality and performance of the internet with the exception that node size is measured in nanometres and channels are physically separated by up to hundreds or thousands of nanometres. In addition, nodes are assumed to be mobile and rapidly deployable. Nodes (or nanodevices) are expected to be either self-powered or spread in and around the specific location. In a visionary sense, an ultimate application of nanoscale networking would be an automated process, where the nano-nodes are in motion communicating in a complex dynamic environment of living organisms monitoring diseased or sensitive parts of the body.

Chapter 1

Smart Nanotextiles for Communication

[1]Isidoro Ibanez-Labiano, [2]Syeda Fizzah Jilani, [3]Ronald Rui Zhang, [4]Elif Ozden-Yenigun, [1]Akram Alomainy

1 School of Electronic Engineering and Computer Science, Queen Mary University of London, London, UK
2 Frontier Institute for Research in Sensor Technologies, University of Maine, USA
3 Beijing Institute of Technology, China
*4 School of Design, Textiles, Royal College of Art, London, UK*

1.1 Introduction

One interesting feature proposed for the future wireless networks is terahertz (THz) (i.e. $0.1 - 10$ THz) communication. When compared to millimetre-wave (mm-wave) communication, THz signals provide higher link directionality and higher security. However, the increased attenuation is a critical limitation at THz than mm-waves, which can be handled by designing shorter-distance and ultra-dense networks probably residing within a building area for the advanced wireless systems. THz communication allows implementation of wireless nano-communication networks comprising of a network of wirelessly connected nano-machines. Given the development of nanotechnology and recent advances in novel materials like carbon nanotubes and graphene, nano-scale antennas designed for THz bands can be manufactured on nano-machines in future. Nano-networks are also anticipated to enable Internet-of-Nano-Things (IoNT) for numerous applications such as environment monitoring, diagnosis services in healthcare, industrial manufacturing, lab-on-a-chip, connected mobility and many smart city applications. For instance, clinical diagnosis and real-time monitoring to ensure patient's well-being by using smart wearables designed on nano-textiles integrated with smart nano-networks are key advantages in this regard.

1.1.1. Nano-communications

We currently live in the age of information, where we gather data from almost every source. In this context, sharing that collected knowledge through communications has turned into a crucial service. Communications have been constantly evolving and expanding thanks to the development of new materials and advanced technologies. These progresses have allowed accommodating new challenging requirements, opening room for new applications at the same time. Among these advancements, wearable wireless devices can play a defining role in the development of a wide range of emerging applications, such as sports analytics [1], wellbeing and health monitoring [2, 3], or positioning systems [4]. Generally, wearable wireless technology will have some form of

communications capability, such as mobile communications, Bluetooth, or Wi-Fi that will allow the wearer to share and access to information in real-time. Features of wearable technology have pushed it to the forefront of the Internet of Things (IoT) and in recent 5th generation of wireless systems (5G) and beyond, where these are expected to play an integral role. 5G networks and beyond are suggested as the future of wireless communication and anticipated to bring high capacity and bandwidth, less latency, ultra-fast communications, a massive number of devices, and long battery lifetime. All this enclosed in compact devices, thus more capabilities on a smaller scale are achieved by tuning materials in nanoscale. Nanotechnology enables nano-communications, where data is exchanged wired or wirelessly at the nano-scale [5]. The deployment of this technology will help with the continuous growth of IoT, evolving into the Internet of Nano-Things (IoNT). Nano-communications will expand the capabilities of nanoengineering and they will extend the range of their applications in several bands of the electromagnetic spectrum.

Communication methods have been adapted for tackling numerous human interactions in body-centric techniques within various applications. New advances in these methods ranging from the ultra-high frequencies (UHF), millimetre-waves from 5G and ultimately to the terahertz (THz) bands are regarded as a key to develop and adjust novel methods to body-centric networks (wearable and implantable). Wireless body area networks (BAN) have been entered into a new generation of wireless sensor networks (WSNs) focused on healthcare monitoring applications, covering various scenarios such as wearable, implantable, or epidermal. This implies that the real-time monitoring of data is envisioned as a transformative approach to wearable applications, especially within the healthcare domain. It is important to understand the performance and behaviour of the channel [6], to study these nano-communications in a hierarchical body area nano-network (BANN) and wireless nano sensor networks (WNSNs). A wireless nano network (WNN) architecture with the essential components and communication links is presented in the Figure 1.
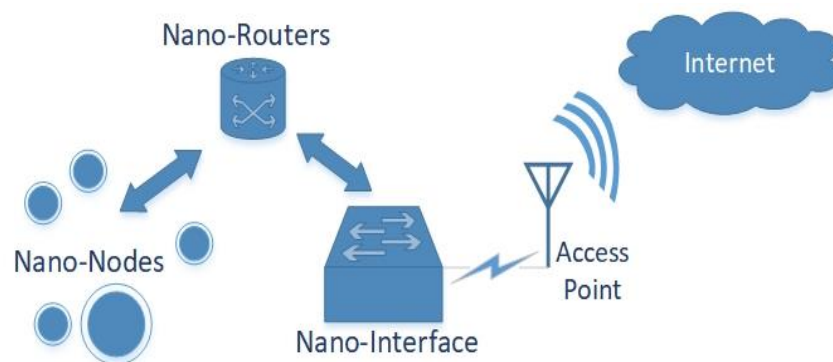
Figure 1. Wireless nano-network architecture.

Where it is essential to understand the channel requirements and constraints, it is crucial to examine the impact of antennas in the nano-communication. Antennas are a key component in the electromagnetic (EM) communication. Theoretical, analytical, and experimental analysis within the field of nano-scale EM-based communication are required to tackle the associated challenges.

On the physical layer regarding the medium where the signals are propagated, so proper channel models are critical to consider path loss, noise, and channel capacity for nano-communications. Furthermore, if we add the human body to the communication channel, the complexity increases due to the differences between one human being and another. The unpredictability of this transmission medium and the limit in communication range, make this real-time operation challenging. Nano-EM communication is known as communication through EM radiation based on novel nanomaterials [7]. The latest advancements in graphene-based electronics have opened the door to EM communication among nano-devices in several frequency bands.

The recent progress of the communication technology demands more versatile and challenging specifications on antenna performances. Antennas in communications are the interface between the propagated EM waves and the communication modules (transmitter and/or receiver). In the wearable electronics, these demands become more challenging where antennas are suggested to deal with the radiation distortions in conformal integrations, maintain high performance without affecting the user experience and capable to act as passive sensors without the need for a battery or any maintenance. In a wearable environment, antennas must be compact, low-profile, and planar structures. New designs should explore solutions using flexible materials, remaining ergonomic and comfortable, but offering mechanical robustness at the same time. Nanoantenna can be made of either conventional metallic materials or novel materials stemming in different carbon allotropes. Among these materials, graphene is the most promising eco-friendly option for these types of material solutions [8, 9].

1.1.2. Smart textiles communications

Smart textiles communications cover a wide range of systems such as Near-field communication (NFC), Bluetooth or Radio frequency identification (RFID), and frequencies within microwaves spectrum. Figure 2 shows a wireless network architecture for the WNSNs which depicts that the nano-node network integrated in a smart clothing that exchanges the information to the wearer's environment from a wireless device such as a smartphone or a wearable gadget through an interface.
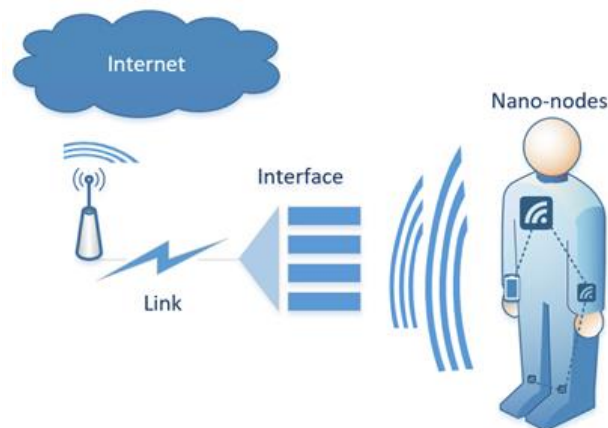

Figure 2. Wireless nano-network architecture for WNSNs.

Communication devices may be easily worn in the future if can be smoothly embedded into the textiles. Wired connections, conductive yarns and optical fibres suit perfectly in the context of e-textiles and can be seamlessly integrated into clothes. These technologies are essential for the development of engineered devices such as sensors and actuators. Enabled wireless communications are required to achieve a more extended environment. This can be completed by integrating an antenna onto the fabrics, for an ease of wearing with several advantages of textile materials [10-11]. However, when coupled with the textiles for the wearable devices several factors will have an impact on the performance. The textile antennas will suffer from the dynamic environment around wearable devices, with physical deformations, wrinkles, strain and bending. Antenna designs should consider these conditions and predict their effects, and materials should present good overall performance without affecting user comfort. Furthermore, there are external factors that cause changes in the fabrics' properties [13]. The fabric's moisture absorption increases the dielectric constant value (ε_r) thus increasing its dimensions (substrate's thickness) [13]. So, relative humidity has a dual impact; a variation in ε_r as well as mechanical deformation. Temperature is a critical parameter in several fields and has a complex and important effect on textiles properties. Increasing temperature in solid materials allows the dipoles freer movement with less control, leading to an increase in permittivity. Around this idea, several versatile antennas have been developed and characterised to be employed as a temperature sensor [14].

The future and perspectives of smart textiles communications are always challenging, but their potential is huge with almost endless applications. Novel materials, antenna designs, fabrication methods and characterization processes will be explored to cope with advanced requirements. This anticipates transformation of a well-established sector as the textile industry into a high-technological business of wearable electronics. This approach demands a cooperation between professionals from various backgrounds and fields of studies. Interdisciplinary teams will boost the possibilities of smart nano-textile communications.

1.2 Textile Wearable Devices

1.2.1. Nano-engineered textile antennas and their applications: Nanoparticles on textiles

Nanotechnology brings an enormously promising and favourable perspective for the textile industry starting from the fibre to the finishes. It has a huge potential which has attracted a lot of attention of many scientists, researchers and businesses. Materials for nano-engineered textile antennas, such as metallic and optical fibres, conductive threads, yarns, conductive coatings and inks are developed to create wireless textile devices. These materials could be split into metallic and non-metallic and could be cast off several forms such as coated layers or fibres.

Conductive inks are having a major impact on the technological advancement of applications within flexible and printable electronics. However, the substrate properties and surface characteristics play an integral role in the ink formulation and performance. Therefore, there must be a suitability between conductive inks and textile substrates, to guarantee optimal performance.

1.2.1.1. Characteristics of metallic inks and fibres

Metallic inks and printed layers are formulated solutions with metallic nanoparticles that attach to the surface of the printed substrate as the ink dries and cured. Silver, gold, aluminium and copper are the most common elements that are included in these inks. Synthesizing these metallic inks is a challenging process that involves mainly three consecutive steps; that starts with the synthesis of the nanoparticles, and continues with formulating a homogenous and stable suspension and finally the implantation based on adaption.

Among these many metallic materials, silver based inks are the most popular due to their high conductivity, $0.4 \sim 2.5 \times 10^7$ S/m [15] and ease in scalable fabrication, and shielding silver particles not to become oxidized quickly. The silver nanoparticles, that are in average diameter of 30 nm, are dispersed at 20 wt% in a solvent. The resolution of the ink deposition becomes critical to avoid over deposition and ensure good surface coverage. Metallic fibres, as another form of conductive form, are either coated by metals such as aluminium, copper, nickel, stainless steel, and silver or use them as the core conduct electrons.

(a)   (b)
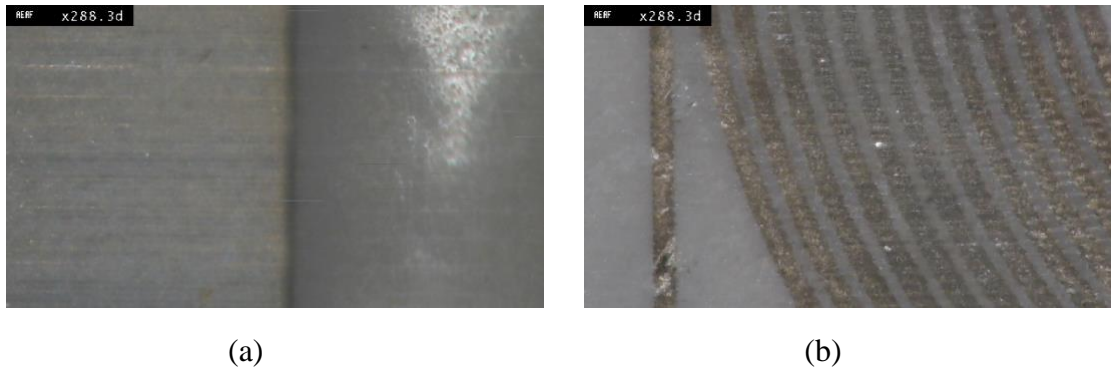
Figure 3. Magnified image of (a) sharp edge of rectangular shape (b) silver inkjet-printed patterns.

1.2.1.2. Characteristics of non-metallic carbon-based inks and fibres

Carbon-based inks have found a prominent role in flexible and printed electronics [16,17]. They are composed of different carbon allotropes, such as carbon black, graphene, carbon nanotubes and graphene nanoflakes. These inks can be formulated to achieve a wide range of electrical conductivity by changing the concentration and form of the conductive carbon particles or by introducing post-processes such as compression. Other advantages of carbon based inks are grounded in the nature of high resistance to abrasion, scratching, flexing, and creasing. Carbon based inks are environment friendly, while still offering superior chemical, mechanical, optical and electrical at a comparable overall performance.

There has been an exciting development in nanotechnology by utilizing carbon nanofibers [18,19]. Graphite/Graphene nanofibers (GNF) and carbon nanotubes (CNTs) can be manufactured using multiple processes and techniques. CNT is among the most researched topics in this field due to its promising results in strength and conductivity in comparison with other carbon nanofibers.

Carbon-based solutions for smart nano-textile communications are popular as these fabrics are anti-bacterial, water-repellent, flame-retardant, ultraviolet-light blocking, have heat and moisture control, wrinkle-resistant, and self-cleaning.

1.2.2. Integration processes for smart nano-textiles (metallic and non-metallic materials)

For both cases, i.e. metallic and non-metallic materials, there are three main techniques of integrating devices onto clothing. First, well-established methods to integrate within the textile industry such as weaving, knitting and embroidering of conductive yarns and threads [20]. Second, conductive sheets lamination process by bonding these films with a fabric substrate [14]. Finally, another common technique is coating the textile with nanoparticles by new additive printing methods, screen or inkjet printing [21].

1.2.3. Smart textile antennas

1.2.3.1. Graphene-soft antenna

The ever-growing number of wireless devices and especially body-centric gadgets has motivated the research to focus on the utilisation of new materials such as Graphene [22]. Using fabrics as substrates for antennas will facilitate their integration in wearable electronics. This section proposes a graphene-based antenna on a textile substrate as a potential candidate for state-of-the-art smart textiles [23].

An UWB antenna with a CPW feed and a planar inverted cone-shaped patch geometry with designed dimensions is shown in Figure 4 (a) with the fabricated prototype in Figure 4 (b). The antenna design was based on the monopole disc principles [24], and the final antenna geometry was obtained from an optimisation process. A chemical vapour deposition (CVD) grown multi-layer (ML) graphene pattern was transferred onto a fabric substrate using a very thin adhesive layer of Ethylene Vinyl Acetate (EVA). For increasing the accuracy, the multi-layer (ML) graphene on polyethene (PE) pattern and alignment mould were trimmed using a vinyl cutter. Finally, a standard 50 Ω SMA connector was bonded to the antenna using a silver-based conductive epoxy (SPI Silver Conductive Epoxy 05000-AB) curable at room temperature. Materials were characterised using a four-probe method for the sheet resistance of ML graphene on the polyethylene (PE) (25 Ω/sq) and a resonant perturbation split cylinder for material characterisation (Agilent 85072A) at 10 GHz with the Keysight material characterization software (N1500A-003 Materials Measurement Suite 2015) for the dielectric properties of the cotton substrate (dielectric constant εr of 1.58 and a dissipation factor (DF) of 0.02).
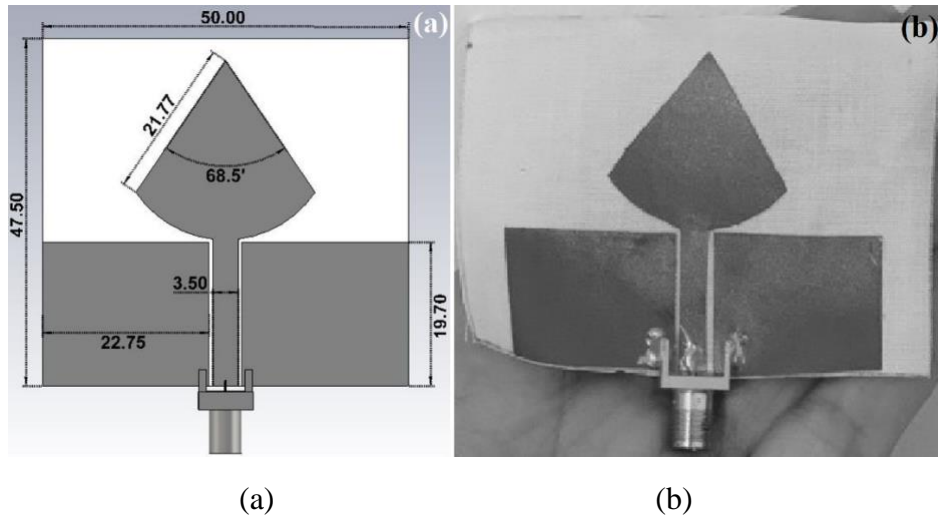
Figure 4. Graphene-soft antenna (a) CAD model with dimensions in mm; (b) Fabricated prototype on cotton [19].

A numerical analysis was carried out using CST-Microwave Studio Suite [25] to evaluate the time-domain characteristics of the antenna structure, in both off-body and on-body conditions. For these simulations, the different layers and the SMA connector were considered. Furthermore, a 44 mm thick four-layer body phantom model was modelled; where the skin, fat and muscle layers were 1 mm, 3 mm and 40 mm respectively. The reflection coefficient (S_{11} parameters) for the four cases considered are represented in Figure 5 below. The antenna shows an operational bandwidth range below -10 dB from 3 to 9 GHz with multiple resonant frequencies. Slight mismatches in the results are due to fabrication tolerances and unavoidable real-time losses during testing.
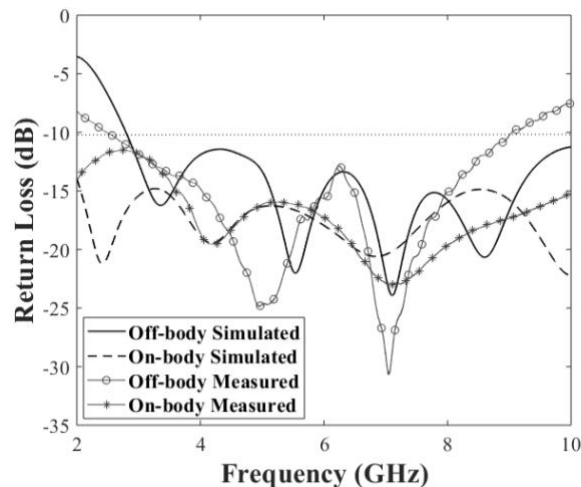

Figure 5. Simulated vs Measured S_{11} of graphene-based antennas in off- and on-body settings [23].

As the antenna is designed to be worn, some extra analyses have been carried out to tackle some of the challenges of a dynamic wearable environment. The impact of washability has been numerically analysed as well as the bending effects for two radii that simulate the average size of

human limbs (70 mm arm and 150 mm leg). Two foam cylinders with ε_r equal to 1 were used to measure the bending effect alone.

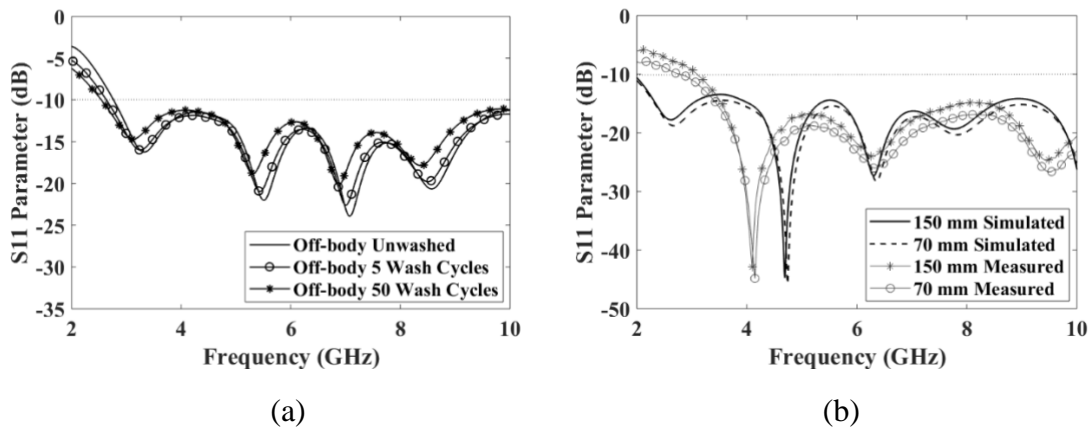(a)   (b)

Figure 6. Simulated vs Measured S_{11} of graphene-based antennas in off- and on-body settings [23].

Washing the antenna has an impact on its sheet resistance, increasing its value with the increment of washing cycles (from 25 Ω/sq unwashed to 50 Ω/sq and 120 Ω/sq, for 5 and 50 wash cycles respectively). Figure 6 (b) shows how bending emphasises one of the resonant frequencies and a slight frequency of detuning was noted for the measured case.

Far-field radiation simulated (black), together with measurements (light grey) for the free-space scenario is presented in Figure 7. Frequencies 3, 5 and 7 GHz have been chosen to represent electric field E-plane ($\varphi = 90°$) and magnetic field H-plane cuts ($\varphi = 0°$) in the full band. Measurements results correlated well with the numerical simulations. It can be considered an omnidirectional pattern as expected, due to its design consisting of a monopole with CPW. As the antenna dimensions were optimised for the lower frequency (i.e. 3 GHz), slightly distorted omnidirectional pattern was observed for the two higher frequencies (i.e. 5 and 7 GHz).
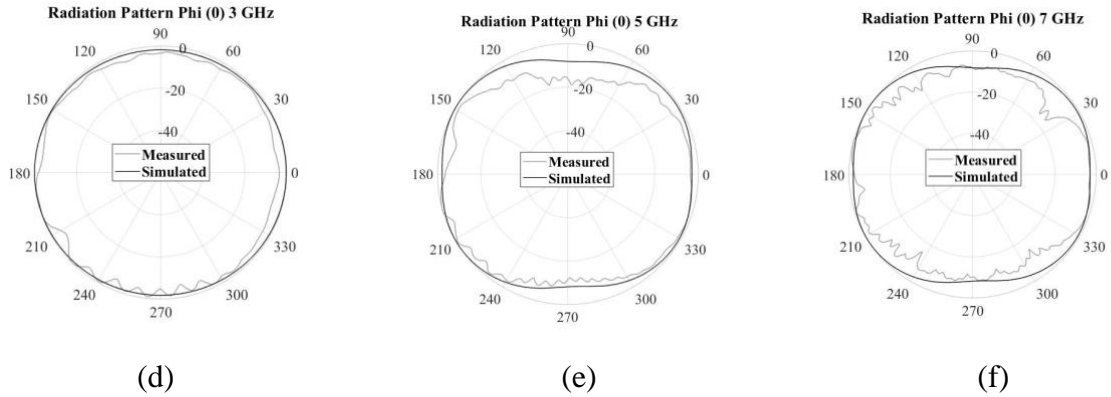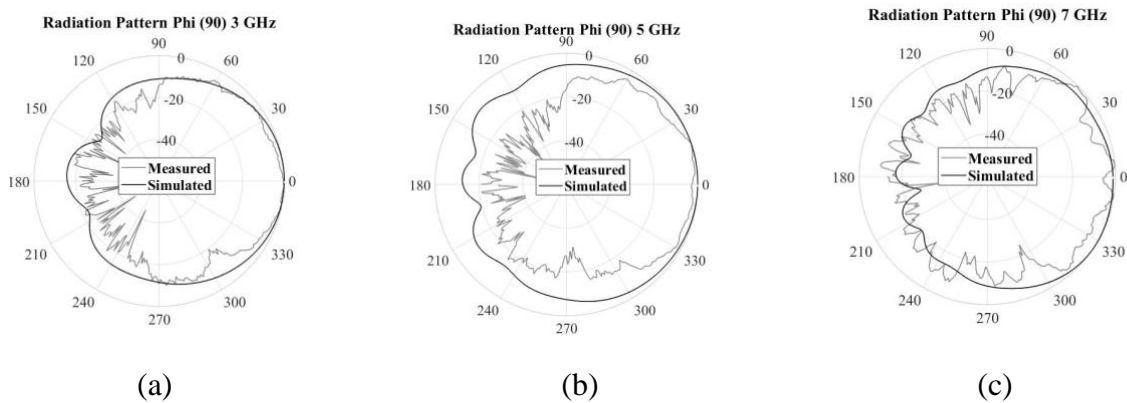

(a)   (b)   (c)
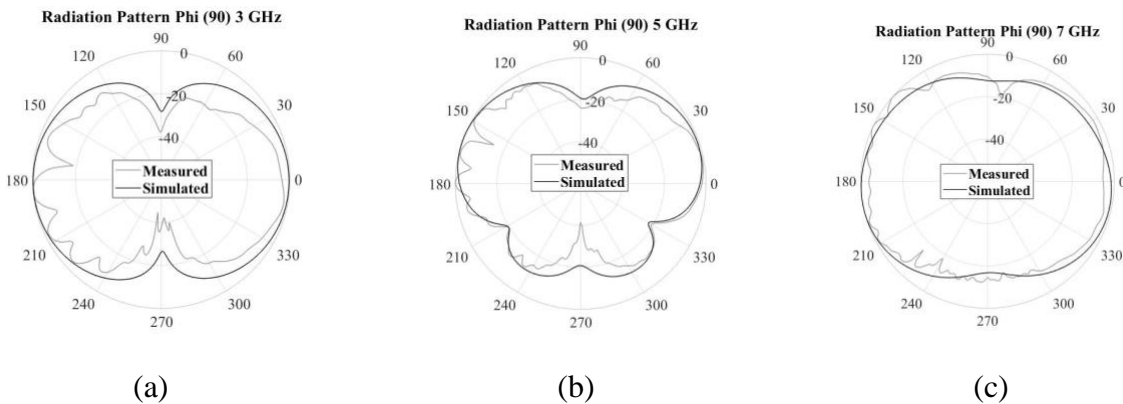
Figure 7. Measured vs simulated radiation pattern of the graphene-based textile antenna in free space at: E-plane cut, at φ = 90°: (a) 3 GHz, (b) 5 GHz and (c) 7 GHz; H-plane cut, at φ = 0°: (d) 3 GHz, (e) 5 GHz and (f) 7 GHz [23].

A second analysis has been carried out to analyse the impact of human body in the antenna's radiation profile. For the numerical simulations, the same previous four layers phantom was used. Regarding the test campaign, a phantom's chest filled with a solution to mimic human tissue properties were practiced evaluating the radiation properties of the antenna on a phantom with no arms and legs. Figure 8 shows the three main frequencies are chosen, 3, 5 and 7 GHz for the on-body cases. Due to the antenna not being isolated with a background plane the presence of the human phantom has a strong impact on the radiation performance in comparison with the free-space situation. The human body absorbs the reflected waves and increases the front-to-back ratio, showing a directional radiation pattern towards the broadside. The variation in the measured results relative to the simulated outcomes is due to the complexity associated with an accurate replication of the human body and intricated properties.
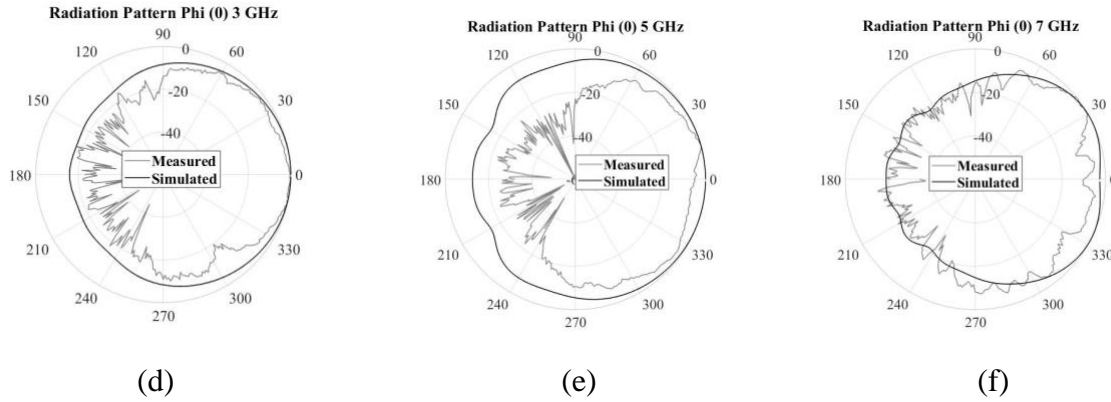
Radiation Pattern Phi (0) 3 GHz   **Radiation Pattern Phi (0) 5 GHz**   **Radiation Pattern Phi (0) 7 GHz**

(d)   (e)   (f)

Figure 8. Measured vs simulated radiation pattern of the proposed graphene-based antenna on the phantom at: E-plane cut, at φ = 90˚: (a) 3 GHz, (b) 5 GHz and (c) 7 GHz; H-plane cut, at φ = 0˚: (d) 3 GHz, (e) 5 GHz and (f) 7 GHz [23].

These results have shown that the CVD grown ML graphene antenna onto a textile substrate has been proven as a successful design for nano-communications as an alternative to metals. This design ensures user-friendliness and unobtrusive integration of technology into electronic textiles. In summary, the proposed textile antenna offers significant structural advantages, such as lightness and washability, along with an operational bandwidth of 6 GHz and an omnidirectional radiation pattern.

1.2.3.2. Inkjet-Printed Millimetre-Wave PET-Based Flexible Antenna

Electronic devices and antennas compatible for conformal integrations are essential for 5G wireless architecture, to maximise the feasibility of incorporating numerous smart features in wearable gadgets for the compact, robust, and reliable user experience [26]. The 5G mm-wave network demands efficient, adaptive, and flexible antennas at the wireless frontends which has encouraged the deployment of many advanced techniques of antenna design on flexible and conformal substrates. So far, several versatile textiles such as polymers, polyimides, polyesters [27], and ultra-thin conformal films of polyethene terephthalate (PET) and Kapton have been successfully used as substrates for printed antennas [28, 29]. For accurate fabrication of the radiating metal part of the antenna, screen printing, photolithography and inkjet printing and embroidery by conductive yarn have been deployed in several antenna configurations [20, 30].

For instance, this antenna aggregates two advanced schemes of efficient spectrum utilisation i.e. frequency-reconfiguration and multiple-input-multiple-output (MIMO) on a flexible substrate to offer compatibility with the 5G wearables. A slotted T-shaped patch along with the reconfiguring switches is designed on a 135 µm thick flexible PET substrate (dielectric constant (ε_r) = 3.2, loss tangent ($\tan\delta$) = 0.002, and dimensions of 11 × 25.4 mm^2) [31]. A rectangular aperture in the ground of the coplanar waveguide (CPW) feed is for the placement of an antenna. Two symmetrical pairs of slots terminated with switches were designed for the desired frequency reconfiguration based on the state of the switches. For x-pair of switches, the antenna resonates at 28-GHz when both the switches are OFF as the slot-edges act as an open-circuit. While the

resonant frequency band shifts to 38-GHz when both switches are ON, the radiating length is trimmed off as the slot-edges act as a short circuit. Another two distinct operating modes were obtained from y-pair of switches. In order to diversify the functionality of the designed antenna as a standalone transmitter and a receiver, a two-element MIMO assembly is presented. Figure 9 shows the design geometry of the MIMO antenna, and dimensions are given in Table 1. Additionally, while implementing the actual switches (e.g., PIN diodes), a biasing circuit is needed to alter the switch-state. Thus, if the x-/y-switch is applied with a potential difference, the metal short parallel to the switch, denoted by z in Figure 9 (a), would provide a path for the direct current (DC), and the switch would not be enabled. A gap of 0.1 mm is inserted at z, along with a 0.1 µF capacitor, which blocks the DC from z without interrupting the AC flow and the DC is directed through the switch.

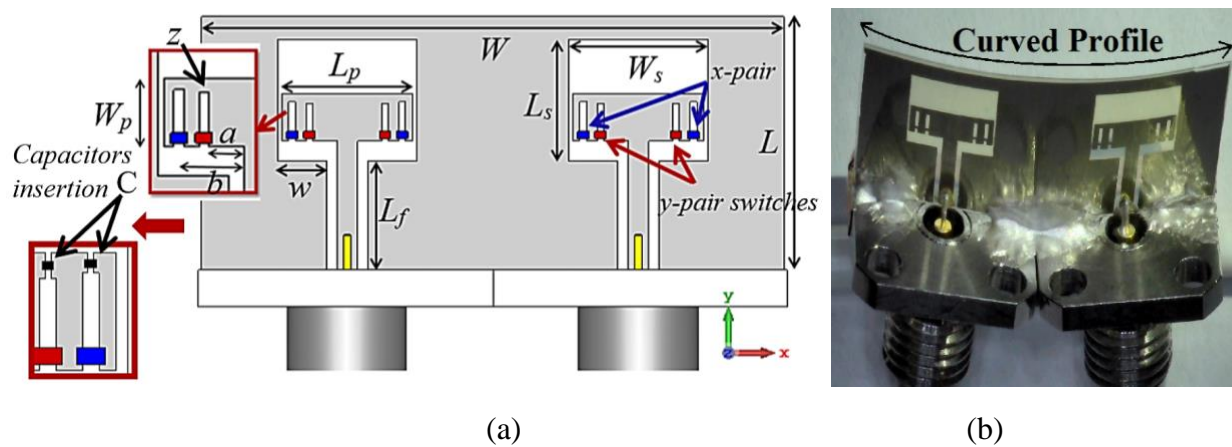(a)   (b)

Figure 9. Proposed flexible frequency-reconfigurable two-element MIMO antenna: (a) simulated antenna model; (b) conformal MIMO antenna [31].

Table 1. Dimensions of the Design Parameters of the Flexible 5G MIMO Antenna.

| Symbol	Parameters	(mm)
L_p	Length of T-shaped patch	5.7
W_p	Width of T-shaped patch	2.05
L_s	Length of ground slot	5.3
W_s	Width of ground slot	6.1
L	Length of 2-element MIMO antenna	11
W	Width of 2-element MIMO antenna	25.4
a	Distance of slot-1 from the feed	1.05
b	Distance of slot-2 from the feed	1.8

L_f	Length of CPW ground	4.7
w	Extended width of the ground slot from CPW	2.15

Inkjet printing is use for antenna prototyping by a Dimatix materials printer (DMP-2831) with the silver nanoparticle ink (i.e., Colloidal Ag-J solid Ag from Printed Electronics Ltd.). The conductive ink is manufactured in such a way that the silver nanoparticles are encapsulated in an organic polymer coating to prevent oxidation and are dispersed in an inert solvent. The ink is composed of a 20.3 % of silver content by weight, suspended in a solution of water (40–50 %), glycerol (30–40 %), and acetylene glycol (0.1–1.0 %). The selected silver ink has a viscosity of 4.2 mPa.s, surface tension of 30.5 mN/m, and density of 1.22 g/cm^3. The post-printing processes of drying, curing, and sintering are essential to release the silver particles from the polymer sheath and combine them into a firm and evenly distributed conductive layer. The conductivity of the sintered silver layer is $0.4 \sim 2.5 \times 10^7$ S/m, and depends on the number of printing iterations, layer thickness, curing temperature, and sintering time durations. Thus, careful sintering could result in conductivity of $0.3 \sim 0.7 \times 10^7$ S/m from a single printed layer. To accomplish the fabrication, the printer was calibrated with a drop-spacing of 15 µm (i.e., 1693.33 dpi), firing voltage of 15 V, and a jetting frequency of 5-KHz. The variation in the surface profile of PET is characterised by using a profilometer, as shown in Figure 10 (a), and utilised while adjusting the printhead position before starting the printing process. A conductive layer with a thickness of 0.5 µm is deposited on a PET film with a pattern resolution of ±20 µm.

The selected PET substrates from Mitsubishi Paper Mills Ltd. are provided with a chemically active microporous adhesive coating to enable the rapid drying and chemical sintering of the ink. This chemical method avoids other sintering methods that involve laser exposure or high-temperature treatments that may result in the bending, shrinking, decolourisation, or even melting of the PET sheet if the temperature is not properly handled. The microporous coating elevates the surface energy of the PET and improves the adhesion by chemically bonding the ink particles with the surface molecules that limits the ink flow outside the pattern to enable precise prototyping. This chemical coating replaces the actual PET surface with a microporous surface that allows partial diffusion of silver nanoparticles for better locking between the ink and the surface, which results in a high adhesion and prevents the layer from peeling off.

The conformal assembly of the designed antenna involves bending of the prototype which may cause cracking of the printed layer with time. Printed layer thickness is critical in this regard as thicker metal layers are more brittle and can be easily cracked by successive bending and folding. For instance, the screen-printed layer is usually 10–20 µm thick with relatively larger sized metallic particles that makes it more brittle and prone to cracks than the inkjet-printed nanoparticle layer which is 0.5 µm thick. To characterise the flexibility of the printed layer, the antenna is firmly mounted on a cylindrical surface of 0.8 mm. Microscopic inspection shows no cracks after bending. To examine the robustness, the conventional scotch tape test is performed [32, 33]. The

tape is adhered to the printed pattern and then peeled off while the printed trace remains fully intact on the substrate which validates excellent ink adhesion and robustness. The prototype is also found water-resistant when submerged in water. Scanning Electron Microscope (SEM) imaging of the printed silver pattern of the antenna is performed to obtain a clear insight which shows a well-formed and closely packed granular nature of the ink layer depicted in Figures 10 (b) and (c).

(a)   (b)   (c)
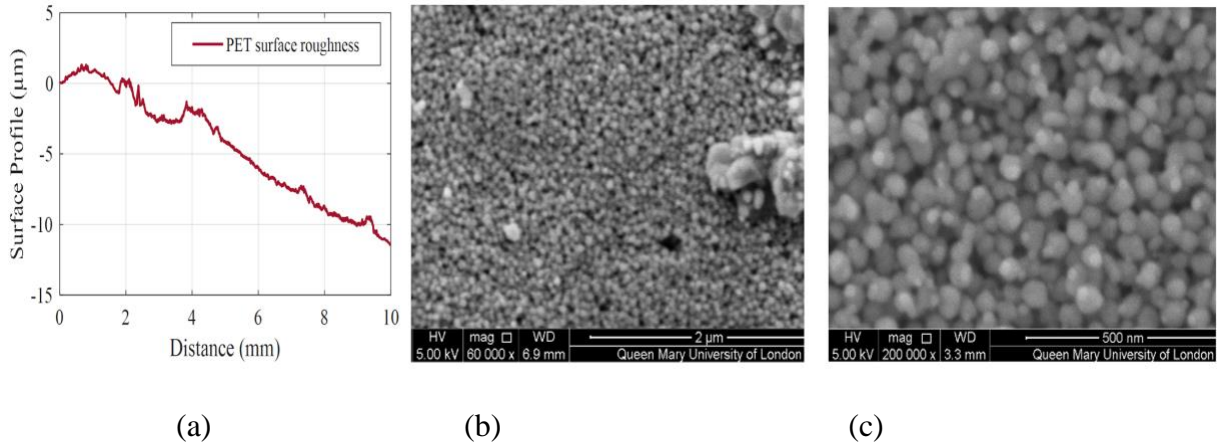
Figure 10. Characterisation of the inkjet-printed antenna prototype, (a) surface profile of PET substrate by profilometer measurements; (b) SEM image of the nanoparticle ink at 4 µm resolution; (c) SEM image of nanoparticle ink at 500 nm resolution [31].

To examine the antenna response toward conformity, the fabricated flexible MIMO antenna is mounted on K-connectors in both planar and conformal configurations (on a curved surface of radius = 3 cm). Figure 11 presents the measured results of the reflection coefficient (i.e., S_{11}/S_{22}) plots for the planar and conformal antenna at four switching modes covering an overall bandwidth of 27.3–40 GHz as shown in Table 2. In a MIMO antenna, each element operates individually thus, the peak gain of a single antenna is more significant than the gain profile of a collective array. The simulated (sim.) and measured (mea.) peak gain magnitudes for a single antenna of the MIMO in the range of 28–40 GHz is tabulated in Table 2 for the operating modes I–IV.
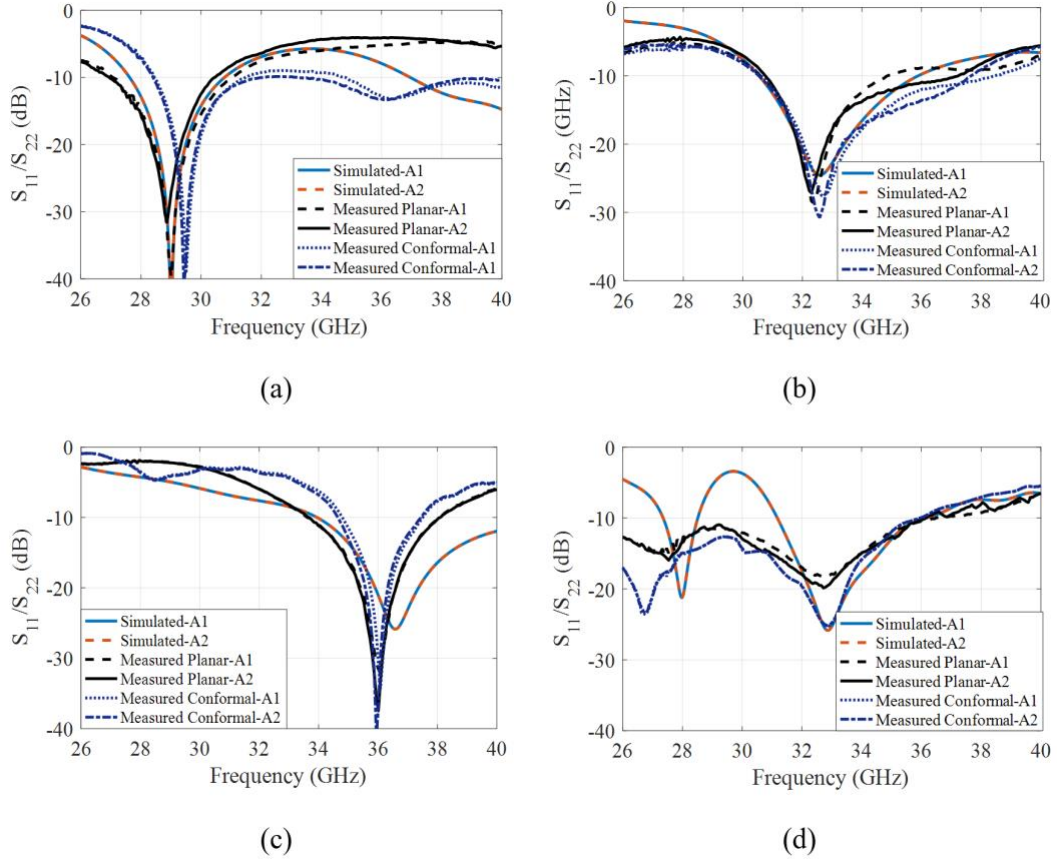
Figure 11. Simulated and measured S_{11}/S_{22} plots of the mm-wave frequency-reconfigurable two-element (i.e., A1 and A2) MIMO antenna: (a) mode-I; (b) mode-II; (c) mode-III; (d) mode-IV [31].

Table 2. Realised Gain at Switch Configurations of the Flexible 5G MIMO antenna.

Mode	SW-x	SW-y	Band (GHz)	BW (GHz)	Gain	Gain (dBi) at distinct frequencies (GHz)						
						28	30	32	34	36	38	40
Mode-I	OFF	ON	28	27.4–30.1	Sim.	2.7	3.8	--	--	--	--	--
					Mea.	2.5	3.4	--	--	--	--	--
Mode-II	ON	OFF	33	30.5–35.9	Sim.	--	--	4.6	3.7	--	--	--
					Mea.	--	--	4.4	3.4	--	--	--

Mode-III	ON	ON	37–39	34–40	Sim.	--	--	--	6.5	4.7	4.2	4.4
					Mea.	--	--	--	6.2	4.6	4.1	4.2
Mode-IV	OFF	OFF	Dual band	27.3–28.5 31.1–36	Sim.	2.7	--	4.3	3.7	5.2	--	--
					Mea.	2.5	--	4.2	3.5	4.9	--	--

The standard spacing between the adjacent elements of an array to avoid mutual coupling should be in-between $\lambda/2$ to λ, , i.e., higher the distance lower the coupling; however, increasing the distance might result in grating lobes [34, 35]. The optimal level of the isolation suggests the transmission coefficients of at least –10 dB or below. The parametric study for high isolation showed that the optimal distance between the centres should be approximately 11 mm (i.e., equals to λ at 27.2-GHz that is the lower cut-off frequency). However, the distance between the centres is slightly increased to 12.7 mm in this proposed MIMO antenna, to accomplish a high isolation below –20 dB in Figure 12 (a). The envelope correlation coefficient (ρe) is computed to evaluate the independence of the antenna elements for their individual operation in a MIMO assembly. Figure 12 (b) presents the low values of the numerically estimated ρe of the MIMO antenna, which depicts the insignificant influence of the adjacent element on the single antenna performance.

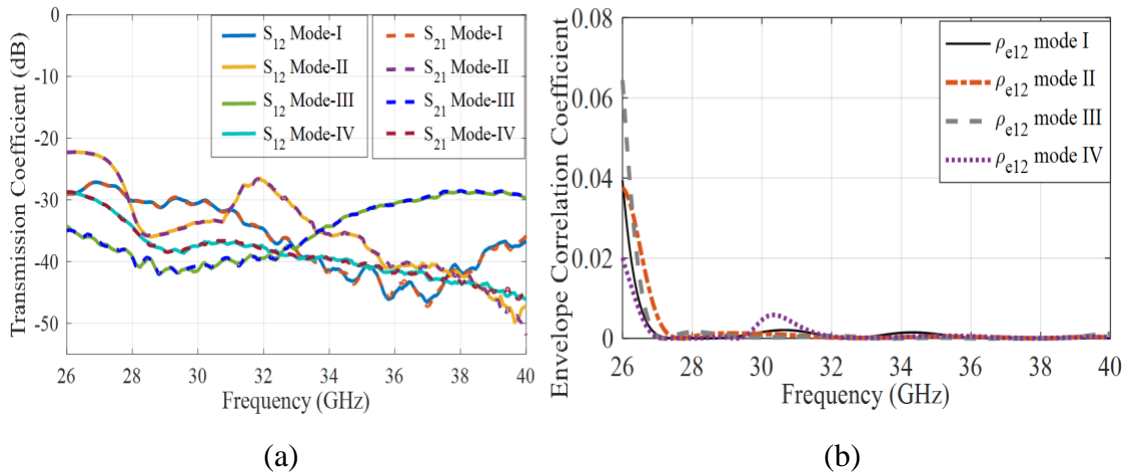(a)   (b)

Figure 12. Mutual coupling analysis of the flexible mm-wave frequency-reconfigurable MIMO antenna for four distinct modes; (a) Measured transmission coefficients (S12 /S21), (b) Simulated envelope correlation coefficient [31].

The radiation characteristics of the developed antenna are measured by using the NSI near-field scanning setup consisting of a precise near-field to a far-field algorithm to compute the far-field radiation patterns. An evenly distributed pattern on the front and bottom with the maximum directivity perpendicular to the surface of the antenna has been observed throughout the operating

range. Figure 13 presents the simulated and measured results of a single element (i.e., a unit cell of the MIMO) distinct frequencies of the operating modes I–IV. As the radiating patch resides in the aperture cut inside the ground plane, it causes the surrounding metallic ground to act as a loop that confines the radiation of the patch orthogonal to the antenna plane (i.e., along with the front and back directions), while the radiation is partially trimmed off along the antenna axis, as shown by the two orthogonal cuts (i.e., E- and H-planes).
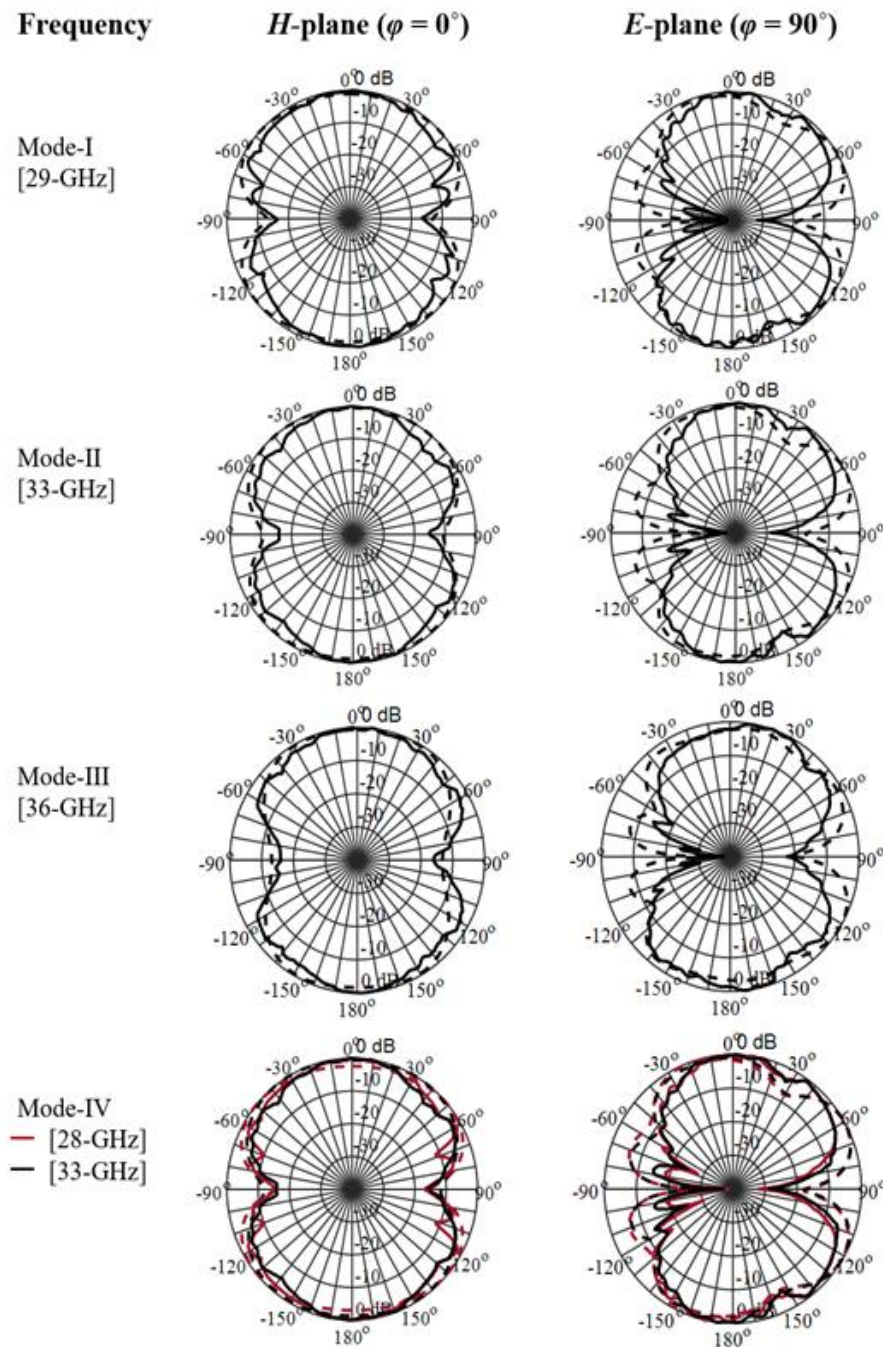

Figure 13. Simulated and measured normalized radiation patterns of the mm-wave flexible single antenna (unit-cell) of the MIMO (i.e. --- Simulated — Measured) [31].

1.2.3.3. Tera-Hertz wearable antenna

The antenna design becomes more complex for body-centric application than the free-space at Terahertz range. The wearable antenna performance could be affected due to presence of human body, as the radiation can be absorbed by the body thus results in lower antenna efficiency. Human skin is a heterogeneous and anisotropic medium and its computational modelling is highly challenging to perfectly integrate all the variables and functions that can affect the EM analysis. The human skin is usually modelled as a 3-layer structure, i.e. epidermis (thickness= 0.05 to 1.5 mm, dermis (1.5-4 mm), and hypodermis (no typical value) [36]. The epidermis contains two layers stratum corneum with only dead squamous cells and the living epidermis layer, where most of the skin pigmentation stay. The stratum corneum is a thin accumulated on the skin outer surface as shown Figure 14. Tera-Hertz band offer high compactness and for fabricating lightweight, thin and low-cost flexible antennas graphene is an excellent choice [37].

The proposed graphene-based antenna is designed and analysed using CST Microwave Studio at the room temperature of 293 K. The rectangular patch of area 260µm × 195µm and a thickness of (0.35×2)nm (i.e. two layers of graphene), with a feedline of 120µm × 100µm of same thickness is designed [38]. The substrate properties such as dielectric constant and thickness govern the radiation characteristics of the antenna. Rogers 3006 is used as substrate with thickness of 175 µm ($\varepsilon_r = 6.5$, $\tan\delta = 0.002$). The antenna is characterised by performance variables such as efficiency, gain, and directivity under free space as well as on-body conditions. The reflection coefficient (S_{11}) of the designed antenna in Figure 14 shows a wide bandwidth of 29.2 GHz, though the plot in on-body state is shifted slightly towards the right side of the 648.2GHz resonance frequency. This deviation is due to the impact of high dielectric constant of the three layers of human body, thus most of the radiated waves propagate through the body and dissipate as heat that results in a wider -10 dB bandwidth. Figure 14 also shows that due to radiation absorption in the human body, the antenna realised gains decreases from 7.8 dBi to 7.2 dBi.
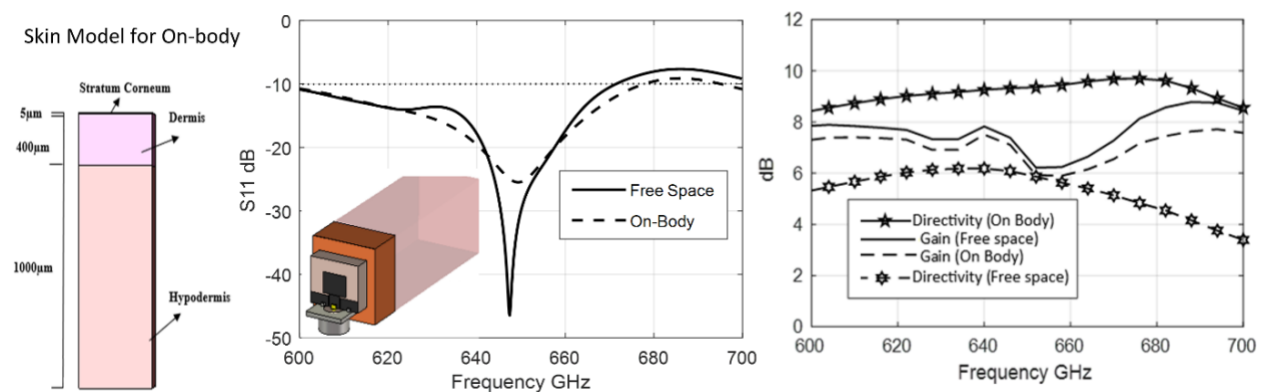

Figure 14. Molecular absorption coefficient as a function of the frequency of human blood, skin and fat [34].

1.3 Nanoscale Body-centric communications

The human body is a great example of a naturally existing communication network. For instance, the nervous system (composed of nerve cells, i.e., neurons) communicates the external stimulus to the brain and enables the communication between different systems by conveying information with a molecular impulse signal known as spike [39-41]. The human body needs communication amongst different cells to survive, the proposed intra- and inter-body nano-scale networks ensure their stability without mechanically (or physically) disturbing the harmony of the in-built molecular structure of the body [42]. The vision of nanoscale networking attempts to achieve the functionality and performance of the internet with the exception that node size is measured in nanometres and channels are physically separated by up to hundreds or thousands of nanometres. The recent progress towards novel materials, like Graphene and its derivatives, namely, Graphene Nano-ribbons (GNRs) and Carbon Nano-tubes (CNTs) [43], encourages the electromagnetic communication among nano-devices in the terahertz (THz) band (0.1-10 THz) due to their ability to slow the propagating wave-making compatible at these frequencies in comparison to the nano-scale. In literature, minimum work on nano-scale communications for in-vivo scenarios applied in healthcare and the use of the THz band as an enabler for such advancement has not been presented or tackled thoroughly, therefore demonstrating the originality and novelty of the research work proposed here.

The modern technology, specifically in bioengineering and bio-electromagnetism dictates in the microwave (50-900MHz) and millimetre wave (30-300 GHz) spectrums and steadily growing in the Terahertz domain [44]. With an increasing awareness of hazardous diseases such as cancer, diabetes and need to improve clinical facilities, the diagnostic research is more focused on extracting intrinsic details of the human body, measurement accuracy and efficient data transfer. THz radiation has gained huge consideration for its extraordinary sensing capability and its non-invasive and non-ionizing features making it a remarkable choice for in-vivo characterisation and imaging of biological systems [44, 45]. The THz spectrum hosts many interesting microscopic phenomena such as inter/intra-molecular motions and Debye relaxation processes. This implies to the ability to use THz radiation for sensing the presence of/or characterise a vast array of materials which are almost inaccessible to other frequency bands. For communication perspective, the THz band channel is highly frequency selective and shows a unique distance-dependent bandwidth behaviour due to the absorption from mainly the content of the biological medium, for instance water and related constituents [46].

An accurate channel model that constitutes the unique biological transmission medium and its associated noise is necessary for the in-vivo THz communication, and the channel capacity that ensures reliable data delivery needs to be assessed. This section presents an analytical model of the THz communication channel for in-vivo nanonetworks by considering the effect of noise on link quality and information rate. The molecular absorption noise model for this THz communication is developed based on the physical mechanisms of the noise present in the human body, which considers both the radiation of the medium and the molecular absorption from the

transmitted signal. To evaluate the link quality, the updated noise model is applied to calculate the signal-to-noise ratio (SNR) of the communication channel for different power allocation schemes. Furthermore, to quantify the potential of the THz band for communication in the human body, the information rate with a single user case has been studied and analysed.

1.3.1 Terahertz Wave Propagation for In-vivo Nanonetworks

1.3.1.1 Theoretical and Analytical Considerations

In this section, the analysis of the end-to-end (that includes channel too) channel model including transmission, propagation and reception of the EM wave is performed. Considering the complexity of the real human tissues, two assumptions are made here:

- A spherically symmetric propagation environment is assumed with the receiver at the centre of the sphere and the transmitter at the distance r from the receiver.
- The antennas of the transmitter are assumed to be ideal isotropic ones.

1.3.1.2 Molecular Absorption

Molecular absorption is a process that the EM energy is partially transformed to kinetic energy internal to vibrating molecules [47], which can be described by the absorption coefficient. Because the vibration frequencies at which a given molecule resonates, change with the internal structure of the molecule [47], this quantity depends on the frequency and gives the THz band a unique frequency-selective spectral absorption profile. Given the absorption coefficient, the amount of incident EM radiation that is capable of propagating through the absorbing medium at a given frequency can be calculated. This parameter is defined by transmittance, which is obtained by using the Beer-Lamberts law as [48, 49],

$$\tau(r, f) = e^{-\alpha(f)r} \tag{1}$$

where f is the frequency of the EM wave, r stands for the total path length and $\alpha(f)$ is the absorption coefficient. Molecular absorption causes attenuation to signals, which can be obtained from the transmittance of the medium τ given by $\tau{r,f} = e^{-\alpha(f)r}$, when travelling a distance r as [47, 50],

$$A_{abs}(r, f) = \frac{1}{\tau(r,f)} = e^{\alpha(f)r} \tag{2}$$

In this research, the communication medium for iWNSNs focuses on human blood, skin and fat tissues and their absorption coefficient at the frequency band of interest are shown in Figure 15. The details on the calculation of the absorption coefficient for human blood, skin and fat tissues can be found in [45, 51]. Compared to the absorption coefficient of water vapour provided in [47], on the one hand, the absorption coefficient in human tissues can be thousands of times than that in the air at the same frequency. Instead, different from the thousand resonant peaks of water vapour over the THz band, the absorption coefficient of human tissues increases with a frequency much more steadily.
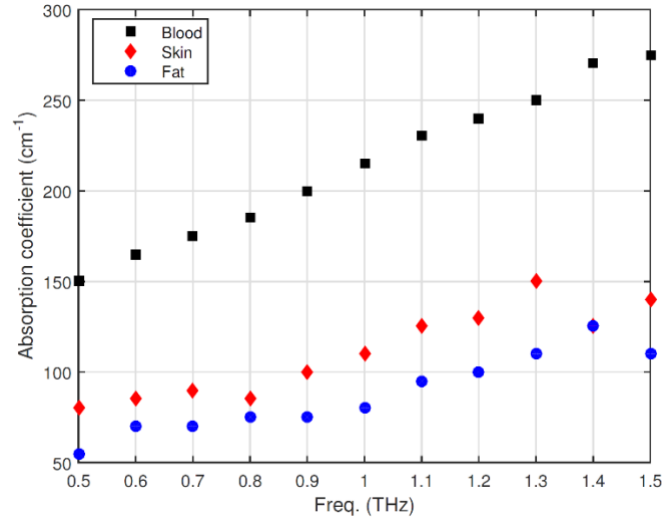
Figure 15. Molecular absorption coefficient as a function of the frequency of human blood, skin and fat.

1.3.1.3 Path Loss

In addition to the molecular absorption, EM waves suffer from the scattering due to the deflection of the beam caused by the microscopic non-uniformities present in the human body. Scattering depends on the particles' diameters and the wavelength of the THz wave. These two parameters help in defining the nature of scattering that the communication will suffer from. Depending on the particles diameter and the wavelength of the THz wave, there are three kinds of scattering as follows:

- Rayleigh scattering (Particles diameter < Wavelength of THz wave)
- Mie scattering (Particles diameter ≈ Wavelength of THz wave)
- Specular and geometric scattering (Particles diameter > Wavelength of THz wave)

The models for scattering by particles and cells in the human body have been analysed and provided in [52]. It is found that the scattering coefficients for human blood and skin are much less than the absorption coefficients at the same frequency. Therefore, compared to the molecular absorption which is the dominant attenuation due to high water content, scattering effect can be neglected in the following study. Thus, the path loss in human tissues can be divided into two components: the spreading loss and molecular absorption loss [51]. The spreading loss is a part of attenuation, caused by the expansion of a wave propagating through the medium and it can be calculated from the modified Friis transmission equation [49],

$$A_{abs}(r,f) = \left(\frac{4\pi nfr}{c}\right)^2 \tag{3}$$

where f is the frequency of the EM wave and n is the corresponding refractive index of the THz wave in the human tissue medium. $4r^2$ denotes the isotropic expansion term and $4\pi(nf/c)^2$ stands

for the frequency-dependent receiver antenna aperture term. Considering the attenuation, the total path loss can be described as,

$$A_{PL}(r,f) = A_{spr}(r,f)A_{abs}(r,f) = \left(\frac{4\pi nfr}{c}\right)^2 e^{\alpha(f)r} \tag{4}$$

and the expected received signal power can be represented by [27],

$$P_R(r) = \int_B S(f)\left(\frac{c}{4\pi nfr}\right)^2 e^{-\alpha(f)r}df \tag{5}$$

The dependency of the channel path loss on the distance and the frequency has also been illustrated in [51]. Due to the considerably high absorption coefficient in human tissues, the path loss suffers more from the molecular absorption loss than the spreading loss. Particularly at the same frequency and transmission distance, the exponential loss due to the molecular absorption is almost double the spreading loss contributions to the path loss. It is demonstrated that the path loss increases with both the transmission distance and frequency and that the path loss would reach 80 dB when the transmission distance increases to 2 mm for all the three different human tissues [51].

It is important to note that even though both Line-of-Sight (LoS) and None-Line- of-Sight (NLoS) propagation schemes can be viable in free space, when it comes to THz communication inside the human body only LoS communication is considered. Because the transmitted signal is significantly attenuated in human tissues and the communication distance is strictly limited, the THz radiation from NLoS coming to the receiver will be negligible.

1.3.2   Molecular Absorption Noise Model

1.3.2.1 Free Space Scenario

The noise in the THz band is primarily contributed by the molecular absorption noise. This kind of noise is caused by vibrating molecules which partially reradiate the energy that has been previously absorbed [47]. Thus, this noise is dependent on the transmitted signal. The total molecular absorption noise p.s.d. SN is proposed to be contributed by the atmospheric noise SN0 and the self-induced noise SN1 in [53], and can be expressed as,

$$S_N(r,f) = S_{N0}(r,f) + S_{N1}(r,f) \tag{6}$$

$$S_{N0}(f) = \lim_{r\to\infty} k_B T_0\left(1 - e^{-\alpha(f)r}\right)\left(\frac{c}{\sqrt{4\pi}f_0}\right)^2 \tag{7}$$

$$S_{N1}(r,f) = S(f)\left(1 - e^{-\alpha(f)r}\right)\left(\frac{c}{\sqrt{4\pi}f_0}\right)^2 \tag{8}$$

where

The atmospheric noise is caused by the temperature of the absorbing atmosphere, making the atmosphere (or any medium) an effective black body radiator in a homogeneously absorbing medium (in the frequency domain) [54]. This atmospheric noise is therefore known as a background noise, which is independent of the transmitted signal. However, the noise model in

$SN0f = \lim\limits_{r\to\infty} k_B T_0 \left(1 - e^{-\alpha(f)r}\right) \left(\frac{c}{\sqrt{4\pi f_0}}\right)^2$ is only a special case for THz communication in air. Without loss of generality, the term $k_B\, T_0$ should be replaced with the Planck's law, since it is a general radiative function of the surface of the black body [54]. Consequently, it is believed that the molecular absorption noise is contributed by the background noise and the self-induced noise.

The background noise caused by the radiation of the medium can be described by the Planck's function [55],

$$B(T_0, f) = \frac{2h\pi f^3}{c^2}\left(e^{\frac{\lambda f}{k_B T_0}} - 1\right)^{-1} \tag{9}$$

where k_B is the Boltzmann's constant and h is the Planck constant. Planck's function is multiplied with π to transform the unit from W/Hz/cm/sr to W/Hz/cm.

For simplicity, the transmission medium is assumed to be an isothermal and a homogeneous layer with the thickness r. As mentioned above, this background noise is generated by the radiation of the local sources of the medium and it is assumed that this radiation is only from the original energy state of the molecules before transmission happens; thus it is independent of the transmitted signal. The background noise can be described as [55],

$$S_{Nb}(f) = \int_0^r B(T_0, f)\alpha(f)e^{-\alpha(f)s}ds = B(T_0, f)\left(1 - e^{-\alpha(f)r}\right) \cong B(T_0, f) \tag{10}$$

The integral $SNb(f) = \int_0^r B(T_0, f)\alpha(f)e^{-\alpha(f)s}ds = B(T_0, f)\left(1 - e^{-\alpha(f)r}\right) \cong B(T_0, f)$ describes the noise intensity at the centre of a sphere with a radius r, given all the points s in the medium contribute to the noise intensity.

In terms of the induction mechanism of the self-induced noise, the internal vibration of the molecules turns into the emission of EM radiation at the same frequency of the incident waves that provoked this motion [47, 52]. It is obtained with the assumption that all the absorbed energy from the transmitted signal received at the receiver would turn into molecular absorption noise as shown in $SN1r, f = S(f)\left(1 - e^{-\alpha(f)r}\right) \left(\frac{c}{\sqrt{4\pi f_0}}\right)^2$, where $(4\pi rf/c)^2$ accounts for the spreading loss.

In

1.3.2.2 In-vivo Scenario

With regards to the in-vivo scenario, the speed of light in the human body could change with the composition of the medium and the frequency of the THz wave. Therefore, c is replaced with c/n
i
n

REF _Ref43295267 \h * MERGEFORMAT $SN(r, f) = S_{N0}(r, f) + S_{N1}(r, f)$

,

R
E

the total molecular absorption noise p.s.d. SN is contributed by the background noise S_{Nb} and the self-induced noise SNs, and can be represented as,

$$S_N(r,f) = S_{Nb}(r) + S_{Ns}(r,f) \tag{11}$$

$$S_{Nb}(f) = B(T_0, f) \left(\frac{c}{\sqrt{4\pi n_0 f_0}} \right)^2 \tag{12}$$

$$S_{Ns}(r,f) = S(f)\left(1 - e^{-\alpha(f)r}\right) \left(\frac{c}{4\pi n r f} \right)^2 \tag{13}$$

where

It is clearly shown that the background noise depends on the temperature and composition of the medium in $SNs(r,f) = S(f)\left(1 - e^{-\alpha(f)r}\right) \left(\frac{c}{4\pi n r f} \right)^2$. It is assumed that the human tissues are iso-thermal; thus, the background noise changes slightly with the refractive index in different transmission mediums. Moreover, the self-induced noise is dependent on the transmitted signal and for simplicity in this section only transmitted signal with flat p.s.d over the entire frequency is considered to comparatively illustrate the difference between these two kinds of noise. To keep the numerical results realistic, and in light of the state of the art in nano-transceivers, the flat power is adopted with the total energy equal to 1 pJ and the pulse duration be 100 fs [59, 60]. The background noise and self-induced noise p.s.d for human blood, skin and fat tissues are in Figure 15 and Figure 16, respectively.

Figure 16 shows that the background noise p.s.d is almost the same in different kinds of tissue because the slight difference of refractive index does not affect much in $SNs(r,f) = S(f)\left(1 - e^{-\alpha(f)r}\right) \left(\frac{c}{4\pi n r f} \right)^2$. Besides, when sharing the same transmitted signal power, the self-induced noise slightly increases from blood to fat, because the absorption coefficient and refractive index increase with the water concentration in the medium and comparatively blood has higher water proportion than skin and fat. More importantly, Figure 17 shows that the noise p.s.d has a steady change with frequency, which is different from the abrupt fluctuation of THz communication in the air as in [47].The reason is that the molecular absorption coefficient has a steady increase over the frequency of interest. Also, the self-induced noise p.s.d decreases with distance. Because the self-induced noise is directly proportional to the transmitted signal, and the signal is inversely proportional to the transmission distance. Thus, the self-induced noise is inversely proportional to the distance.

Moreover, comparing Figure 16 with Figure 17, the self-induced noise p.s.d is about seven orders of magnitude higher than the background noise in all these different human tissues. The main reason is that the transmitted pulse energy is chosen to be high enough for better information transmission. In this case, it can be concluded that the self-induced noise is the dominant noise source and the background noise is negligible in the THz band for in-vivo nano-networks.

The molecular absorption noise p.s.d for these considered tissues is illustrated in Figure 18, which is almost the same as the self-induced noise p.s.d. This highlights the fact that the background noise can be discarded in our analysis.
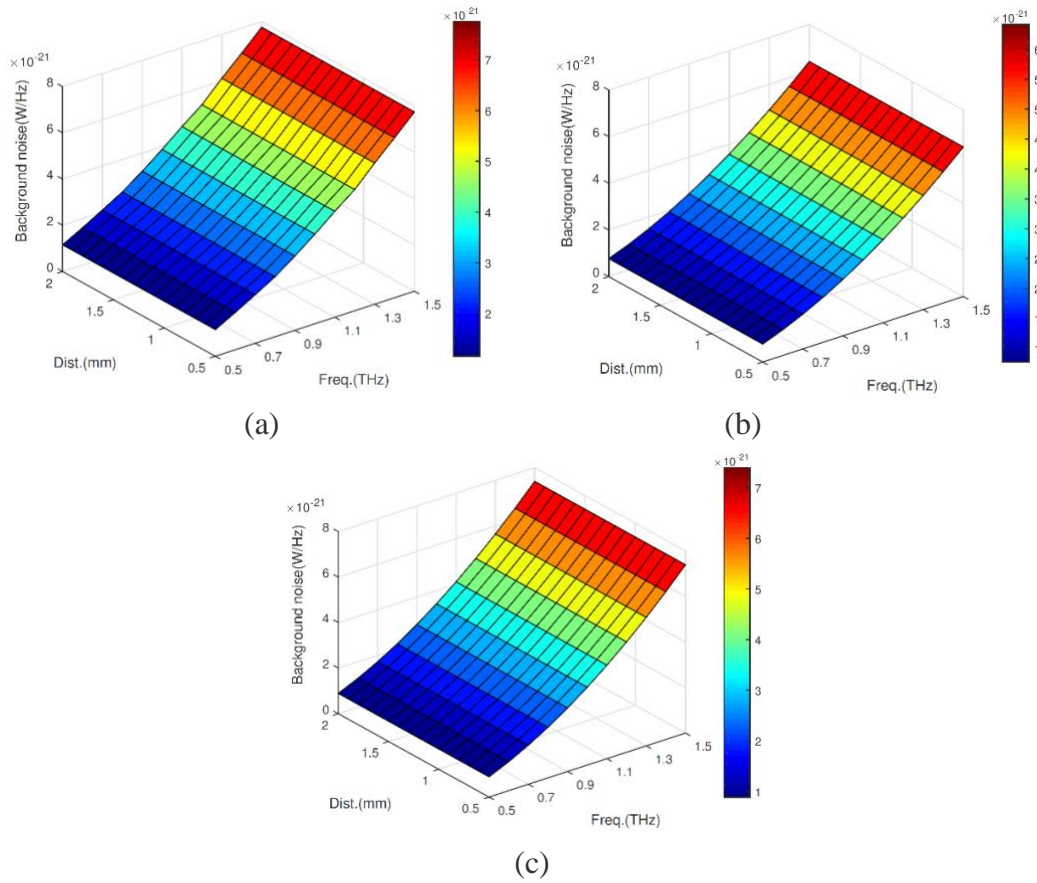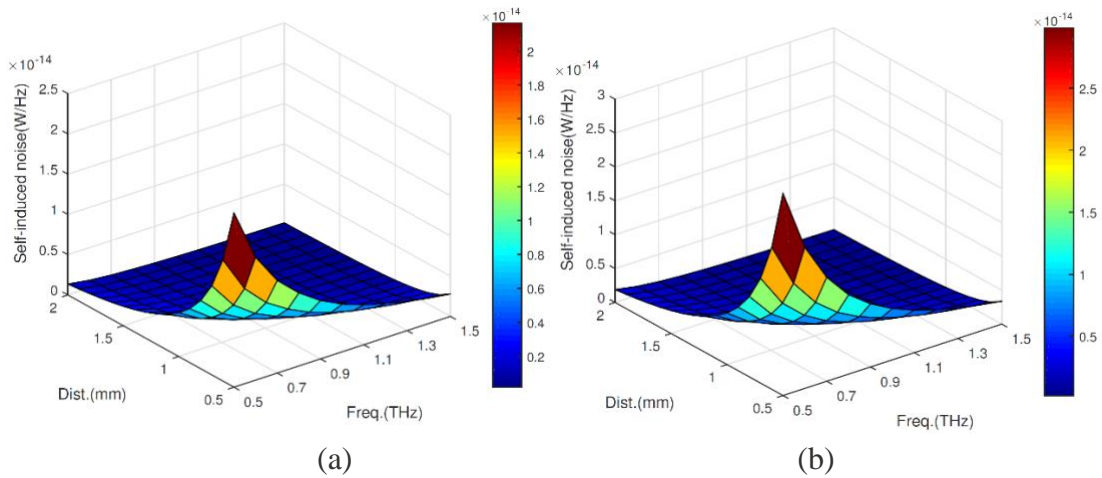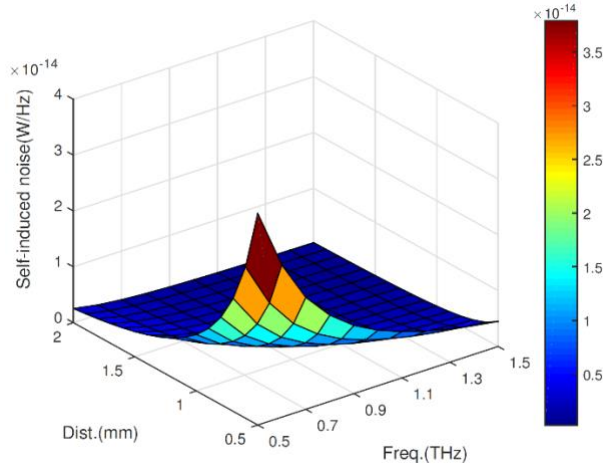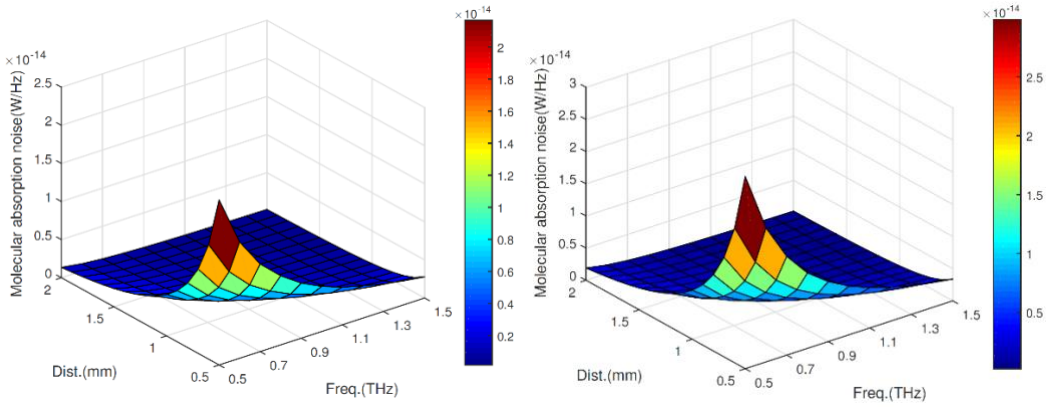

(a)

(b)

(c)

Figure 16. Background noise p.s.d at the THz frequencies for different human tissues (a) Blood, (b) Skin and (c) Fat.
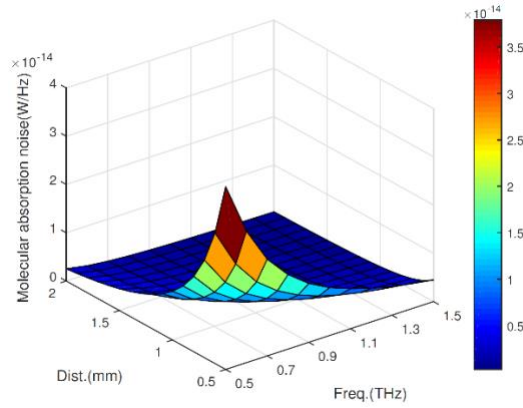

(a)

(b)

(c)

Figure 17. Self-Induced noise p.s.d at the THz frequencies for different human tissues (a) Blood, (b) Skin and (c) Fat.

(a)

(b)

(c)

Figure 18. Molecular absorption noise p.s.d at the THz frequencies for different human tissues (a) Blood, (b) Skin and (c) Fat.

1.4 Challenges and Future Prospects

The interest in smart nano textiles is growing while more applications are being proposed. Nonetheless, there are several challenges to be tackled in such as interdisciplinary knowledge and one of the most important is nano networking. Novel nanotechnology integrated into the fabric of clothes will use these nanonetworks to communicate with each other with the environment. A hurdle in this novel field is the lack of standardization, regulations and common guidelines. Collaboration between different international entities public as well as private has to be encouraged.

Common challenges within communications in general such as bid data handling and privacy are also faced within the smart nano textile world. The smart nanotextiles are expected to deal with a large amount of data interacting simultaneously with several types of communications at different ranges (in-body, on-body and off-body). This fact will have an impact on the power consumption and size of the systems, and consequently in the integration of the communication nano-devices. The importance of cooling systems is increasing, the current capabilities of this area of the communications system are insufficient and need further developments. The integration of nano-communications systems must be automated, where fabrication techniques from the electronic and textile industries should be combined.

All the personal data gathered by the sensors and devices attached to fabrics should be treated and protected, following user constraints about the use, access and storage of data. Security challenges of personal data are quite a huge issue that is a whole topic by itself with several challenges linked to it. Furthermore, smart fabrics should deal in real-time or near real-time with this vast amount of data adding complexity to the networks.

Environmental sustainability is one of the major challenges facing in our current times, reusable fabrics and new materials will help in this direction. However, the proper characterization of these items' full test campaigns should be carried out and more research is needed to develop the new set of smart textiles.

Clothes also face the challenge of user acceptance and durability. Wearable devices need to be designed and tested in order to prove their resilience against effects such as bends, cramps, washing cycles, and so on. Smart textile communications will take into account the above points, but without neglecting product usability and the user's experience. This last point is sometimes disregarded but is extremely important. The challenge is to involve the user in all stages of the process.

The points discussed in previous paragraphs clearly show that there are many gaps that need to be filled within the world of smart nano textiles for communications. These gaps open new research opportunities in different disciplines among scientists and engineers.

1.5 Conclusion

This chapter has focused on the electromagnetic side and communications of smart textiles at a nanoscale. Reviewing materials and processes in order to design and later fabricate smart fabrics prototypes, identifying and highlighting challenges and plausible applications.

Developments in smart nano textiles will impact our daily lives in several aspects by enabling a world of applications unobtrusively for wearers and their environs. The potential applications of smart textile nanonetworks are limitless, such as biomedical, environmental, industrial, or military applications and they will have a great impact in almost every field. New materials will play a key role in the integration of novel technologies, enabling the further expansion of nanonetworks within smart clothing. New materials such as graphene and techniques have been explored in order to comply with the specific requirements of this type of technology.

At the same time, communications of devices at the nanoscale are essential to accomplish more complex tasks. This requirement of smart nanotextile communications will push the development of more advanced nanodevices.

The development of smart nanotextiles communications is promoting the setup of interdisciplinary teams of people from materials science, electrical and electronic engineering, and people from the textile communities. These collaborations will result in new developments based on combining the knowledge and experience from different fields.

In summary, communications of smart nanotextiles are a new paradigm which requires the merging a well-established industry such as the textile with the novel methods the emerging world of nanotechnology.

REFERENCES

[1]. Suh M, Electronic textiles: smart fabrics and wearable technology. Chapter 12 - Wearable sensors for athletes. Woodhead Publishing, 2015.

[2]. Survase SC and Deshmukh VV. Simulation and design of wearable antenna for telemedicine application. Int. J. Advanced Research in Electrical, Electronics and Instrumentation Engineering, 2013;2(5):1977–83.

[3]. Corchia L, Monti G, Benedetto ED and Tarricone L. Wearable antennas for remote health care monitoring systems. Int. J. Antennas Propag., 2017; Article ID:3012341:1–11.

[4]. Singh J, Kalra P, Singh S and Sidhu E. High gain textile rectangular microstrip patch antenna design employing denim substrate for satellite space to earth downlink applications, Int. Conf. Global Trends in Signal Processing, Information Computing and Commun. (ICGTSPICC). 2016;338–43.

[5]. Akyildiz IF, Jornet JM and Pierobon M. Nanonetworks: A new frontier in communications. Commun. ACM, 2011;54(11):84–9.

[6]. Yang K, Pellegrini A, Munoz MO, Brizzi A, Alomainy A. and Hao Y. Numerical analysis and characterization of THz propagation channel for body-centric nano-communications. IEEE Trans. Terahertz Sci Technol, 2015;5(3):419–26.

[7]. Rutherglen C. and Burke P. Nanoelectromagnetics: circuit and electromagnetic properties of carbon nanotubes. Small, 2009;5(8):884–906.

[8]. Kumar J, Basu B, Talukdar FA, and Nandi A. Graphene: A possible low-cost eco-friendly solution for antenna applications. IEEE Applied Electromagnetics Conf. (AEMC) 2017;1–2.

[9]. Scida A, Haque S, Treossi S, et al. Application of graphene-based flexible antennas in consumer electronic devices. Materials Today. 2018;21(3):223–30.

[10]. Priya A, Kumar A, and Chauhan B. A review of textile and cloth fabric wearable antennas. Int. J Computer Applications. 2015;116(17):1–5.

[11]. Rais NHM, Soh PJ, Malek F, Ahmad S, Hashim NBM and Hall PS. A review of wearable antenna. Loughborough Antennas Propagation Conf. (LAPC) 2009;225–28.

[12]. Salvado R, Loss C, Gonçalves R and Pinho P. Textile materials for the design of wearable antennas: A survey. Sensors. 2012;12:15841–57.

[13]. Morton WE and Hearle JWS, Physical properties of textile fibres, 4th Edition. The Textile Institute CRC Press, Woodhead Publishing Limited, 2008.

[14]. Ibanez-Labiano I and Alomainy A. Dielectric characterization of non-conductive fabrics for temperature sensing through resonating antenna structures. Materials. 2020;13(6):1271.

[15]. Yang L, Rida A, Vyas R and Tentzeris MM. RFID tag and RF structures on a paper substrate using inkjet-printing technology. IEEE Trans. Microw. Theory Tech. 2007;55(12):2894–901.

[16]. Secor, E. B., Ahn, B. Y., Gao, T. Z., Lewis, J. A., & Hersam, M. C. Rapid and Versatile Photonic Annealing of Graphene Inks for Flexible Printed Electronics. Advanced Materials, 2015, 27(42), 6683–6688.

[17]. Huang, L., Huang, Y., Liang, J., Wan, X., & Chen, Y. Graphene-based conducting inks for direct inkjet printing of flexible conductive patterns and their applications in electric circuits and chemical sensors. Nano Research, 2011, 4(7), 675-684.

[18]. Jinho H, Dong WP and Sang ES. A Review on Thermal Conductivity of Polymer Composites Using Carbon-Based Fillers : Carbon Nanotubes and Carbon Fibers. Carbon Letters 2010, Vol. 11, No. 4, pp. 347-356.

[19]. Wang, J., & Musameh, M. Carbon nanotube screen-printed electrochemical sensors. The Analyst, 2004, 129(1), 1.

[20]. Andrade, AdC, Fonseca IP, Jilani SF and Alomainy A. Reconfigurable textile-based ultra-wideband antenna for wearable applications. 10th European Conf. Antennas Propag. (EuCAP). 2016:1–4.

[21]. Jilani SF, Munoz MO, Abbasi QH and Alomainy A, Millimeter-wave liquid crystal polymer based conformal antenna array for 5G applications. IEEE Antennas Wireless Propag. Lett. 2019;18(1):84-8.

[22]. Palacios T, Hsu A and Wang H. Applications of graphene devices in RF communications. IEEE Commun. Mag. 2010;48(6):122–8.

[23]. Ibanez-Labiano I, Ergoktas MS, Kocabas C, Toomey A, Alomainy A, Ozden-Yenigun E. Graphene-based soft wearable antennas. Applied Materials Today, Volume 20, 2020, 100727, ISSN 2352-9407.

[24]. Liang J, Guo L, Chiau CC, Chen X and Parini CG. Study of CPW-fed circular disc monopole antenna for ultra wideband applications. IEE Proceedings - Microwaves, Antennas and Propagation, 2005;152(6), 520-526.

[25]. CST Simulation Software

[26]. Elobaid HAE, Rahim SKA, Himdi M, Castel X and Kasgari MA. A transparent and flexible polymer-fabric tissue UWB antenna for future wireless networks. IEEE Antennas Wireless Propag. Lett. 2017;16:1333–6

[27]. Tehrani BK, Cook BS and Tentzeris MM. Inkjet printing of multilayer millimeter-wave Yagi-Uda antennas on flexible substrates. IEEE Antennas Wireless Propag. Lett. 2016;15:143–6

[28]. Saeed SM, Balanis CA and Birtcher CR. Inkjet-printed flexible reconfigurable antenna for conformal WLAN/WiMAX wireless devices. IEEE Antennas Wireless Propag. Lett. 2016;15:1979–82

[29]. Li X, Sidén J and Andersson H. 2018 Flexible circuits and materials for large-area UHF RFID reader antenna systems Flex. Print. Electron. 2018;3 (1):015005

[30]. Jilani SF, Abbasi QH, Imran MA and Alomainy A. Design and analysis of millimetre wave antennas for the 5th generation networks and beyond. in Tafazolli, R., Wang, C.-

L. and Chatzimisios, P. (Eds.) Wiley 5G REF: The Essential 5G Reference Online. Wiley. ISBN 9781119471509

[31]. Jilani SF, Rahimian A, Alfadhl A and Alomainy A. Flexible and low-profile inkjet-printed frequency-reconfigurable millimeter-wave MIMO antenna for 5G applications. Flexible and Printed Electronics-IOPscience, 2018;3:035003.

[32]. Sridhar A, J Reiding J, Adelaar H, Achterhoek F, van Dijk DJ and R Akkerman R. Inkjet-printing- and electroless-plating-based fabrication of RF circuit structures on high-frequency substrates. J. Micromech. Microeng. 2009;19:085020.

[33]. Fang Y, Hester JGD, Su W, Chow JH, Sitaraman SK and Tentzeris MM. A bio-enabled maximally mild layer-by-layer Kapton surface modification approach for the fabrication of all-inkjet-printed flexible electronic devices. Sci. Rep. 2016;6:39909.

[34]. Rahimian A. Design and performance of a Ku-band Rotman lens beamforming network for satellite systems. Progress In Electromag. Research M. 2013;28:41–55.

[35]. Ahn J, Cha SH, Cha SG, and Yoon YJ. Compact spiral element for wideband beam-steering arrays. IEEE Antennas Wireless Propag. Lett. 2017;16:1994–7.

[36]. Abadal S, Llatser I, Mestres A, Lee H, Alarcon E and Cabellos- Aparicio A. Time-domain analysis of graphene-based miniaturized antennas for ultra-short-range impulse radio communications. IEEE Trans. Commun. 2015;63(4):1470–82.

[37]. Dashti M. and Carey JD. Graphene microstrip patch ultrawide band antennas for THz communications. Advanced Functional Materials. 2018;28(11):1705925.

[38]. Abohmra A, Jilani F, Abbas HT, et al. Flexible and wearable graphene-based terahertz Antenna for body-centric applications. Second Int. Workshop on Mobile Terahertz Systems (IWMTS), 2019;1–4

[39]. Huan-Bang Li, Kenichi Takizawa, and Ryuji Kohno. Trends and standardization of body area network (BAN) for medical healthcare. pages 1–4. IEEE, 2008.

[40]. Abbasi QH, Yang K, Chopra N, Jornet JM, Abuali NA, Qaraqe KA and Alomainy A. Nano-communication for biomedical applications: A review on the state-of-the art from physical layers to novel networking concepts. IEEE Access. 2016;4:3920–35.

[41]. Malak D and Akan OB. Molecular communication nanonetworks inside human body. Nano Communication Networks. 2012;3(1):19–35.

[42]. Akyildiz IF and Jornet JM. Electromagnetic wireless nanosensor networks. Nano Communication Networks. 2010;1(1):3–19.

[43]. Jornet JM and Akyildiz IF. Graphene-based plasmonic nano-antenna for Terahertz band communication in nanonetworks. *IEEE J. Selected Areas in Commun.* 2013;31(12):685–94.

[44]. Yang X, Zhao X, Yang K, et al. Biomedical applications of Terahertz spectroscopy and imaging. Trends in Biotechnology. 2016;34(10),810–24.

[45]. Abbasi QH, Rehman MU, Qaraqe K and Alomainy A. (eds.), Advances in body-centric wireless communication: applications and state-of-the-art, The IET, July 2016.

[46]. P. Boronin, Petrovac V, Moltchanov D, Koucheryavy Y and Jornet JM. Capacity and throughput analysis of nanoscale machine communication through transparency windows in the terahertz band. Nano Communication Networks, 2014;5(3):72–82.

[47]. Jornet JM and Akyildiz IF. Channel modeling and capacity analysis for electromagnetic wireless nanonet-works in the terahertz band. IEEE Trans. Wireless Commun. 2011;10(10):3211–21.

[48]. Paine S. The am atmospheric model (sma tech. memo 152; cambridge: Harvard univ.). 2004.

[49]. Fox M, Optical properties of solids. oxford master series in condensed matter physics. 2001.

[50]. Jornet JM and Akyildiz IF, Channel capacity of electromagnetic nanonetworks in the terahertz band. IEEE Int. Conf. on Commun. 2010;1–6.

[51]. Yang K, Pellegrini A, Munoz MO, Brizzi A, Alomainy A. and Hao Y. Numerical analysis and characterization of thz propagation channel for body-centric nano-Chapter 3. End-to-End Terahertz Communication for In-vivo Wireless Nano-Sensor Networks 74 communications. IEEE Trans. Terahertz Sci. technol. 2015;5(3):419–26.

[52]. Elayan H, Shubair RM and Jornet JM. Bio-electromagnetic thz propagation modeling for in-vivo wireless nanosensor networks. 11th IEEE European Conf. Antennas Propag. (EUCAP), 2017;426–30.

[53]. Wang P, Jornet JM, Malik MA, Akkari N and Akyildiz IF. Energy and spectrum-aware mac protocol for perpetual wireless nanosensor networks in the terahertz band. Ad Hoc Networks, 2013;11(8)2541–55.

[54]. Kokkoniemi J, Lehtoma˙ki J and Juntti M. A discussion on molecular absorption noise in the terahertz band. Nano Communication Networks. 2016;8:35–45.

[55]. S. Chandrasekhar, Radiative transfer. Courier Corporation, 2013.

[56]. P. Boronin, V. Petrov, D. Moltchanov, Y. Koucheryavy, and J. M. Jornet, Capacity and throughput analysis of nanoscale machine communication through transparency windows in the terahertz band. Nano Communication Networks, 2014;5(3):72–82.

[57]. A. K. Geim and K. S. Novoselov, "The rise of graphene," Nature materials, vol. 6, no. 3, pp. 183–191, 2007.

[58]. A. N. Pal and A. Ghosh, "Ultralow noise field-effect transistor from multilayer graphene," Applied Physics Letters, vol. 95, no. 8, p. 082105, 2009.

[59]. J. M. Jornet and I. F. Akyildiz, "Graphene-based plasmonic nano-transceiver for terahertz band communication," in The 8th European Conference on Antennas and Propagation (EuCAP 2014). IEEE, 2014, pp. 492–496.

[60]. V. Ryzhii, M. Ryzhii, V. Mitin, and T. Otsuji, "Toward the creation of terahertz graphene injection laser," Journal of Applied Physics, vol. 110, no. 9, p. 094503, 2011.